IEEE Access
Multidisciplinary | Rapid Review | Open Access Journal

Received October 22, 2021, accepted November 8, 2021, date of publication November 11, 2021,
date of current version November 29, 2021.

Digital Object Identifier 10.1109/ACCESS.2021.3127533

Measurement-Based Electric Arc Furnace Model Using Ellipse Formula

CHOONGMAN LEE[1], (Member, IEEE), HEEJIN KIM[2], (Member, IEEE), EUN-JAE LEE[3], (Member, IEEE), SEUNG-TAEK BAEK[3], (Member, IEEE), AND JAE WOONG SHIM[4], (Member, IEEE)

[1]Korea Railroad Research Institute, Uiwang 16105, South Korea
[2]Pion Electric, Seoul 03722, South Korea
[3]LS Electric, Anyang 14119, South Korea
[4]Department of Electrical Engineering, Sangmyung University, Seoul 03016, South Korea

Corresponding author: Jae Woong Shim (jaewshim@smu.ac.kr)

This work was supported by the National Research Foundation of Korea (NRF) Grant by the Korean Government through MSIT under Grant 2018R1C1B5084745 and Grant 2021R1C1C1012806.

ABSTRACT This paper proposes a mathematical model of an electric arc furnace (EAF) system based on the voltage and current (V–I) field data. The proposed method is formulated using the ellipse equation, which is derived from the measurement profile of real EAF systems. This paper also presents the harmonics and power-pattern information corresponding to the smelting processes (boring, melting, and refining) in order to realistically design an EAF for potential industrial applications. The third harmonic component significantly affects the shape of the V–I curve in realistic EAF systems, while the periodic power fluctuation is closely associated with the size of the ellipse. These characteristics can be formulated and designed by the proposed method, and even in the absence of the V–I profile, an EAF model can be generated using the generalized information provided in this paper. The electrical phenomenon in the proposed method is mathematically verified using the PSCAD/EMTDC software.

INDEX TERMS Electric arc furnace, iron furnace, aluminum furnace, ladle melt furnace, ellipse formula.

I. INTRODUCTION

An electric arc furnace (EAF) generally exhibits random and nonlinear characteristics that cause power quality problems and threaten the stability of the connected power system in severe cases. EAFs are considered as problematic loads with respect to the power quality concerns because of their nonlinear characteristics, resulting in penalty payments for grid-code violations. Specifically, the flicker is a critical concern, as the EAFs irregularly consume large amounts of active and reactive power [1], [2], and the asymmetrical operating condition of the EAF system should be investigated in the transmission system [3]. Additionally, the harmonics from the EAF load is one of the main issue [1], [4]–[6], containing particularly a significant third harmonic component [7]. The interactions with the capacitance and reactance elements in the network is investigated in [8], [9]. To ameliorate these power quality problems, additional compensation equipment such as passive filters [4], [10], active filters [11]–[13] and static VAR compensators (SVCs) are studied [14], [16].

The associate editor coordinating the review of this manuscript and approving it for publication was Shiwei Xia.

Various approaches have been proposed in previous studies to develop a model for the EAF systems to handle the aforementioned issues. Since a simulation model that shows the load characteristics of EAF is essential to analyze the problem through case study [17], [18], existing techniques have been reported such as the voltage–current (V–I) characteristic method [19]–[23], time-domain equivalent nonlinear circuit method [17], [24], and frequency domain analysis for a nonlinear differential equation, and the random and chaotic approaches [24], [25].

Regarding harmonics concerns, numerous approaches have been introduced such as multiple synchronous frame method [11], [26], wavelet transformation [27], Kalman filter [12], spectral optimization [13], and data-driven strategies [11], [28], [29]. To accurately calculate power consumption of EAFs, advanced prediction methods [16], [30], frequency domain estimation [31], and an improved filter-based calculation [15].

Among them, this study focuses on the V–I characterization to develop an EAF model. Previously, V–I curve for each phase is presented in [3], [24] to assess an unbalanced problem due to EAF. Also, references [24], [32] investigate

the power quality issues, including flicker and harmonics with time-domain simulation.

Meanwhile, the measured V–I characteristics of the industry EAF are embodied with time-varying equivalent impedance values in [19], [33]–[35]. This approach is advantageous as it allows for the formation of an impedance model that can handle the power characteristics of the EAF system according to industrial application. Also, this facilitates the analysis of the power system, including aspects such as system protection, oscillation, and resonance issues, since EAF systems involve grid impedance components [8], [9], [36]–[38]. Furthermore, the proposed impedance model can incorporate the characteristics for each manufacturing process (boring, melting, and refining), and it is observed that the proposed model comprehensively simulates the EAF system.

Similar fashion to this V–I modeling method, previous approaches such as stochastic modeling [22], [23], [35], optimization technique [34], and data-training method [21] have provided high-accuracy models to handle various power quality problems associated with EAF; however, these approaches have its own limitation to adjust the model or build a new model due to their unavoidable complex structures. Hence, we propose a method which can create the model by simply applying the measurement data.

The proposed modeling process collects the V–I measurement data and represents the characteristics, including the low-frequency oscillations and harmonics, as the ellipse formula. It provides a mathematical foundation for the EAF system modeling. Furthermore, this study presents a method to form the time-varying impedance model with the given data (in this paper) in the absence of the V–I profile, such as in the planning stage.

The advantages and contributions of the proposed method are summarized as follows:

- Formation of the time-varying impedance model for the detailed manufacturing processes (boring, melting, and refining) associated with the V–I profile of practical EAF systems.
- Establishing a theoretical framework for EAF modeling and creating an ellipse formula including the effects of the low-frequency oscillation and third harmonic components.
- Providing a framework for the EAF system modeling in the absence of the measurement data for the industrial applications.

The remainder of this paper is organized as follows. Section II describes the manufacturing process and the voltage–current characteristics. Section III introduces the development of the EAF model with and without the measurement data and provides a mathematical foundation using the ellipse formula. Section IV presents the case studies to verify the application of the proposed method.

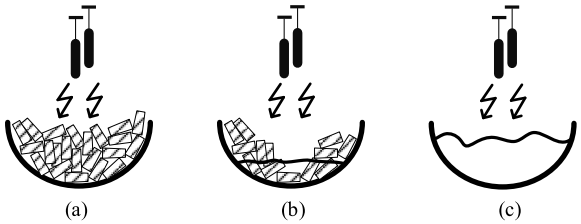

FIGURE 1. The furnace process including three steps (a) boring, (b) melting, and (c) refining.

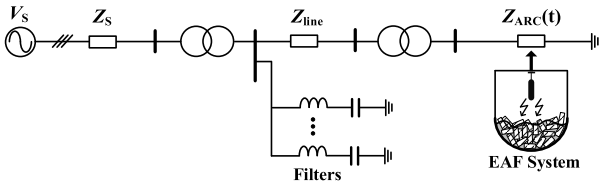

FIGURE 2. The single-line diagram of the network including EAF system represented as the time-varying impedance.

II. DESCRIPTION OF ELECTRIC ARC FURNACE SYSTEM

A. SMELTING PROCESS

Owing to the random nature of an EAF, identifying the pattern of the power consumption is difficult even for the equivalent steel material. Therefore, an EAF model with greater accuracy is required to assess the stability of the power system, including the power quality concerns. In this paper, the furnace types are iron furnace, aluminum furnace, and ladle melt furnace (LF). Moreover, the smelting process is further classified into three processes, i.e., boring, melting, and refining, and a model corresponding to each process is built to describe an accurate load characteristic.

Figure 1 shows the smelting process: boring, melting, and refining. In the first step, the boring process causes severe power quality problems such as significant harmonics and flickers. The melting process is observed to be more stable than the first step; however, the nonstationary currents flow into the network because of the raw materials that have not been completely melted. Lastly, in the refining stage, the arc length and the current magnitude exhibit the least amount of change owing to the liquid materials.

It must also be noted that EAF systems are interfaced with electric power systems. Thus, it is beneficial to develop an impedance model considering all of the above processes owing to the interactions between EAF systems and grid-side impedance components [9], [39].

Consequently, the entire system can be represented as shown in Fig. 2. The filter banks for the harmonic rejection are included in the network. The network embodies the EAF system as the time-varying impedance on the secondary side of the transformer. This study presents the development of the time-varying impedance components corresponding to the type of furnace system and the steps described above.

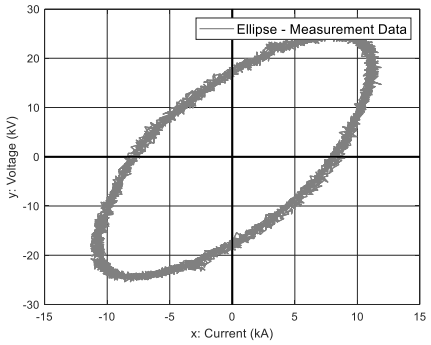

FIGURE 3. V–I curve with field data of existing ladle furnace in South Korea.

B. V–I MEASUREMENT DATA OF AN ACTUAL ARC FURNACE SYSTEM

The availability of a modeling method based on the V–I field data is considered in this section. Firstly, the V–I characteristics of the EAF system are considered for the impedance modeling.

The V–I curve is illustrated as shown in Fig. 3 using the field measurement of an LF in South Korea. The LF has a more stable process when compared to the EAFs, due to which the current and voltage for fundamental frequency exist dominantly among various harmonic components. Therefore, the V–I characteristics approximate the shape of an ideal ellipse.

To establish the mathematical foundation, the magnitude and phase information of the fundamental frequency component is obtained through fast Fourier transforms (FFT). The V–I characteristic is then derived using the obtained information of the fundamental frequency component as follows:

$$\begin{cases} v(t) = \sqrt{2}V_1 \sin(\omega t + \theta_{v1}) \\ i(t) = \sqrt{2}I_1 \sin(\omega t + \theta_{i1}) \end{cases} \quad (1)$$

where V_1, θ_{v1}, I_1, and θ_{i1} are the values obtained through the FFT, and $v(t)$ and $i(t)$ are the voltage and current functions based on the measurement data, respectively.

Figure 4 shows the V–I curve (blue) based on (1) in comparison to the curve (gray) of the measurement data of an existing LF system. It can be stated that the measurement data present the V–I characteristics of the actual EAF since the features of the two ellipses illustrated in Fig. 4 are almost identical. Furthermore, it implies that the EAF system can be simulated with time-varying impedance including the V–I information.

III. ELECTRIC ARC FURNACE MODELS BASED ON ELLIPSE FORMULA

A. IMPEDANCE MODEL BASED ON V–I MEASUREMENT DATA

The characteristics of an existing EAF system are represented as an ellipse with a formula in Section II. Consequently, this study presents a method to formulate a time-varying impedance based on the ellipse formula. The formulation process for time-varying impedance is illustrated in Fig. 5.

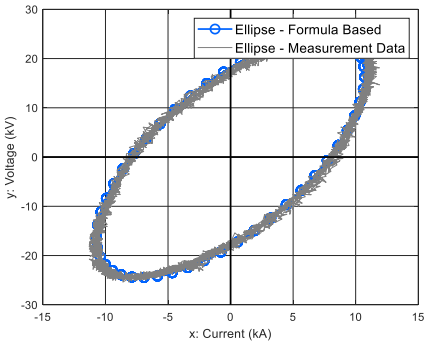

FIGURE 4. V–I curve with field data and the ellipse with FFT data.

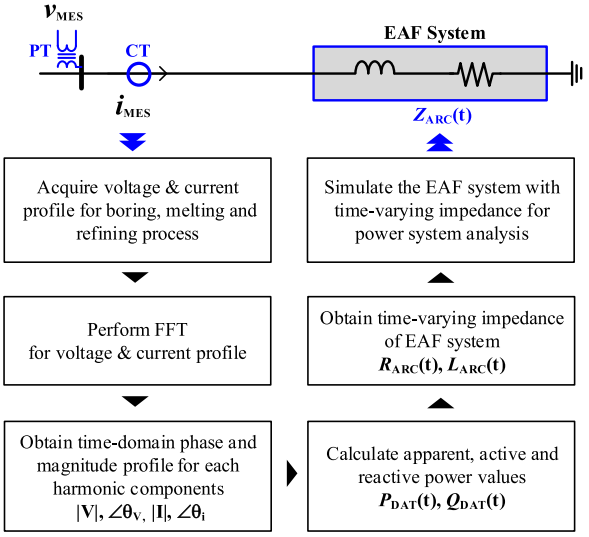

FIGURE 5. Modeling process for the time-varying impedance with V–I measurement data of an actual EAF system.

The profile of the voltage and current must be collected for an actual EAF system in order to form the time-varying impedance as shown in Fig. 6. In this research, we installed a field data measuring equipment on the secondary side of the transformer at an real EAF site in South Korea and measured the voltage and current with the sampling frequency of 100 kHz. Then, based on the real data of EAF voltage and current profiles, we carry out the analysis using PSCAD software and calculate the active power and reactive power, and acquire the harmonic information.

The voltage source behind the impedance in Fig. 6 represents the harmonic voltages occurring inside the furnace. The voltage, v_{harm}, includes the nth-order harmonics, given as follows:

$$v_{harm}(t) = \sum_{h=1}^{n} \sqrt{2}V_h(t) \sin(h\omega t + \theta_h(t)) \quad (2)$$

where V_h, f_h, and θ_h are the values obtained from the V–I profile.

To sum all the harmonic components up to the nth order (up to the 50th in this study), v_{harm} represents the internal harmonic voltage of the EAF systems.

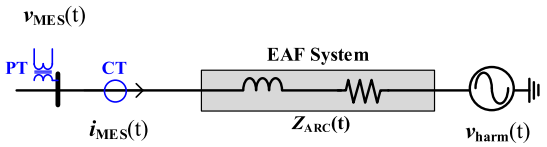

FIGURE 6. The impedance model of EAF system.

The voltage and current functions can then be obtained as follows:

$$\begin{cases} v_{\mathrm{MES}}(t) = \sum_{h=1}^{n} \sqrt{2} V_{\mathrm{h}}(t) \sin(h\omega t + \theta_{\mathrm{v,h}}(t)) \\ i_{\mathrm{MES}}(t) = \sum_{h=1}^{n} \sqrt{2} I_{\mathrm{h}}(t) \sin(h\omega t + \theta_{\mathrm{i,h}}(t)) \end{cases} \tag{3}$$

where V_{h}, I_{h}, $\theta_{\mathrm{v,h}}$, and $\theta_{\mathrm{i,h}}$ are the RMS voltage, RMS current, voltage phase angle, and current phase angle information for each harmonics orders of actual measured data, respectively.

With these obtained information, the phase angle at which the V–I characteristic can be implemented as a formula can be derived in (4).

$$\theta_{\mathrm{ARC,h}}(t) = \theta_{\mathrm{v,h}}(t) - \theta_{\mathrm{i,h}}(t) \tag{4}$$

Based on (3) and (4), the information on the V–I can be reorganized as shown in Fig. 7(a). The power calculation for the EAF is performed using the above equations as follows:

$$\begin{cases} P_{\mathrm{MES}}(t) = \sum_{h=1}^{n} V_{\mathrm{h}}(t) I_{\mathrm{h}}(t) \cos\theta_{\mathrm{ARC,h}}(t) \\ Q_{\mathrm{MES}}(t) = \sum_{h=1}^{n} V_{\mathrm{h}}(t) I_{\mathrm{h}}(t) \sin\theta_{\mathrm{ARC,h}}(t) \end{cases} \tag{5}$$

The active and reactive powers are illustrated with the angle at which the V–I characteristics are implemented, as shown in Fig. 7(b).

Essentially, the active and reactive power values are obtained to produce the time-varying impedance components, including the resistance, $R_{\mathrm{ARC}}(t)$, and the reactance, $X_{\mathrm{ARC}}(t)$.

$$\begin{cases} P_{\mathrm{MES}}(t) = [I_{\mathrm{MES}}(t)\,]^2 R_{\mathrm{ARC}}(t) \\ Q_{\mathrm{MES}}(t) = [I_{\mathrm{MES}}(t)\,]^2 X_{\mathrm{ARC}}(t) \end{cases} \tag{6}$$

where I_{MES} is the RMS components for i_{MES} in (3).

In summary, the time-varying impedance components can be derived as follows using the active and reactive power calculations according to (3)–(6).

$$\begin{cases} R_{\mathrm{ARC}}(t) = \dfrac{P_{\mathrm{MES}}(t)}{[I_{\mathrm{MES}}(t)\,]^2} \\ L_{\mathrm{ARC}}(t) = \dfrac{Q_{\mathrm{MES}}(t)}{\omega[I_{\mathrm{MES}}(t)\,]^2} \end{cases} \tag{7}$$

In other words, the time-varying impedance model of the EAF system can be formed through (3)–(7) based on the field measurement.

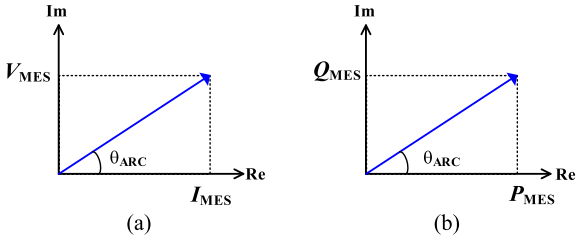

FIGURE 7. V–I coordination and P-Q coordination with the angle of the EAF system.

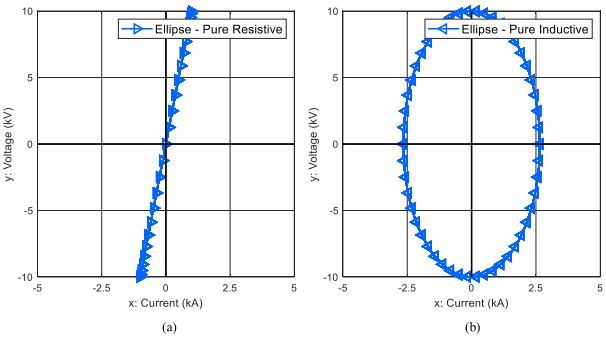

FIGURE 8. Ellipses illustrated by the impedance model configured by (a) pure resistance and (b) pure inductance.

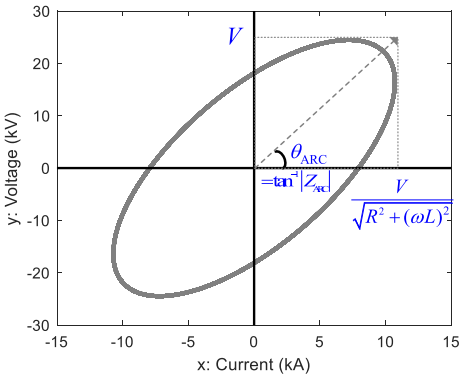

FIGURE 9. Ellipse illustrated by the time-varying impedance model for EAF system.

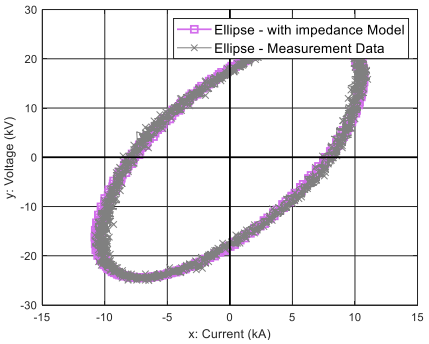

FIGURE 10. Ellipses illustrated by (a) the time-varying impedance model (proposed model) and (b) V–I measurement data.

B. MODELING BASED ON ELLIPSE FORMULA REGULATION

The ellipse consists of the sinusoidal waveform of the current (x-axis) and voltage (y-axis) represented in the Cartesian

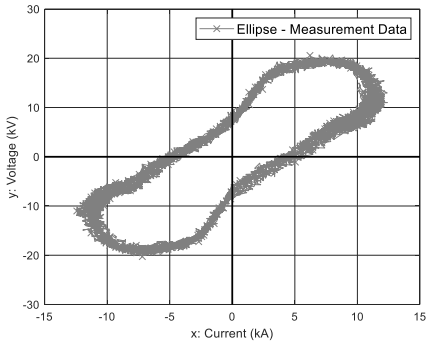

FIGURE 11. Effects of the third harmonics components (ellipse illustrated by V–I measurement data of iron furnace).

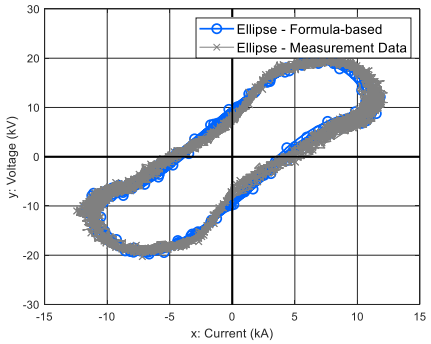

FIGURE 12. Ellipse illustrated by (a) V–I measurement data of iron furnace and (b) FFT data including fundamental frequency and third harmonic elements.

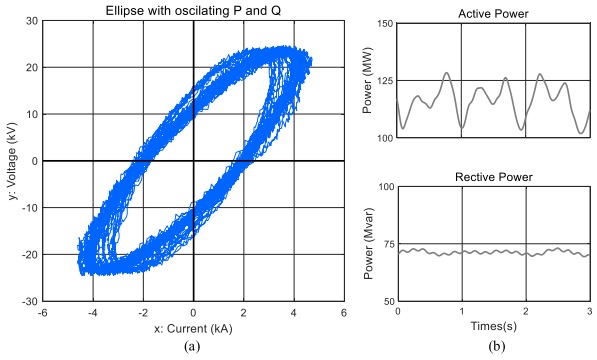

FIGURE 13. Effects of power oscillations: (a) ellipse illustrated by V–I measurement data with power oscillations; (b) power oscillations on active- and reactive power.

coordinates as shown in Fig. 3. To organize (1) into Cartesian coordinates, it can be expressed as follows:

$$\begin{cases} x : i(t) = I\sin(\omega t + \theta_{\mathrm{i}}) \\ y : v(t) = V\sin(\omega t + \theta_{\mathrm{v}}) \end{cases} \tag{8}$$

where I, V, θ_{i} and θ_{v} are the RMS current, RMS voltage, current angle and voltage angle for EAF system, respectively. It facilitates the representation of the V–I characteristics as an ellipse formula when the EAF system is modeled with the time-varying impedance in (7).

Subsequently, the effect of the impedance components on the V–I characteristics, that is, the shape of the illustrated ellipse, is analyzed.

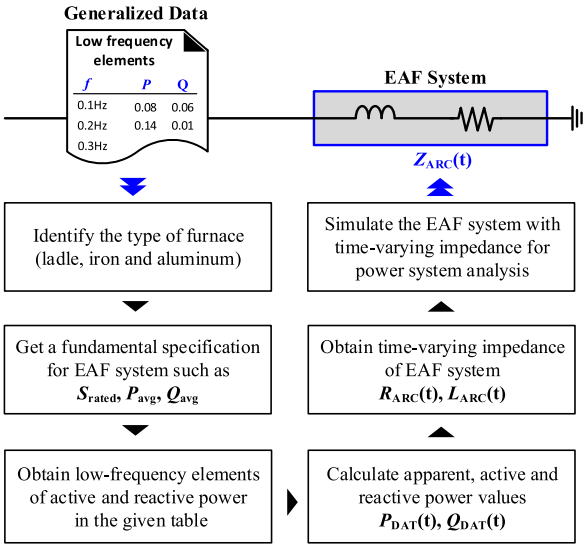

FIGURE 14. Modeling process for time-varying impedance with the generalized data in tables in Appendix (without V–I measurement data).

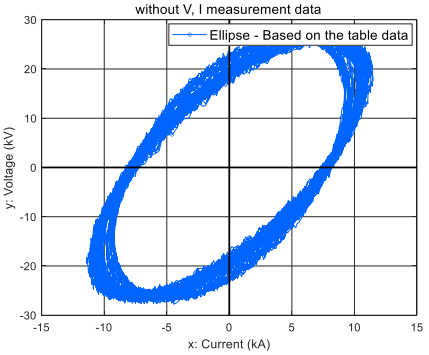

FIGURE 15. Ellipse illustrated by the generalized data in tables in Appendix.

When the time-varying impedance contains only the resistance component, the ellipse is expressed as follows:

$$\begin{cases} x(t) = \dfrac{V}{R}\sin\omega t \\ y(t) = V\sin\omega t \end{cases} \tag{9}$$

The linear V–I characteristics are observed as shown in Fig. 8(a) since the x-axis component and the y-axis component are in the same phase as represented in (9).

As the time-varying impedance contains only the reactance component, the ellipse is expressed as follows:

$$\begin{cases} x(t) = \dfrac{V}{\omega L}\sin(\omega t - 90\,^{\circ}) \\ y(t) = V\sin\omega t \end{cases} \tag{10}$$

A vertical ellipse is observed as shown in Fig. 8(b) since the x-axis component and the y-axis component have a phase difference of 90° as represented in (10).

By incorporating these two components, the ellipse model with the resistance and reactance components is derived as

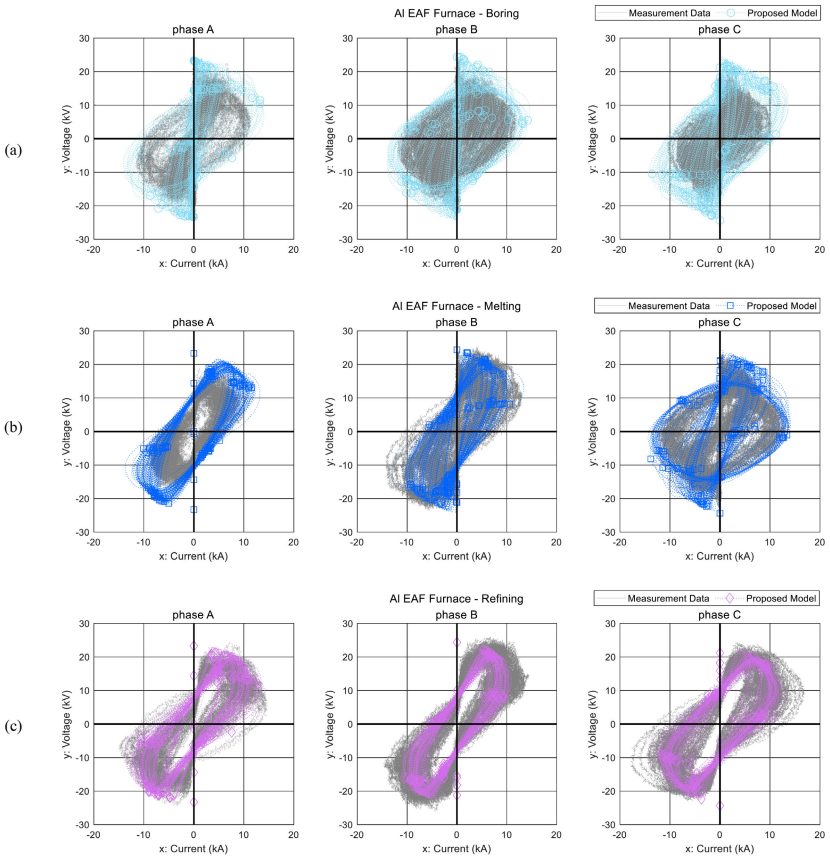

FIGURE 16. Case study result of aluminum furnace system: comparison of the V–I curve (by measurement data) with the ellipse (by the proposed model) for the three steps: (a) boring, (b) melting, and (c) refining.

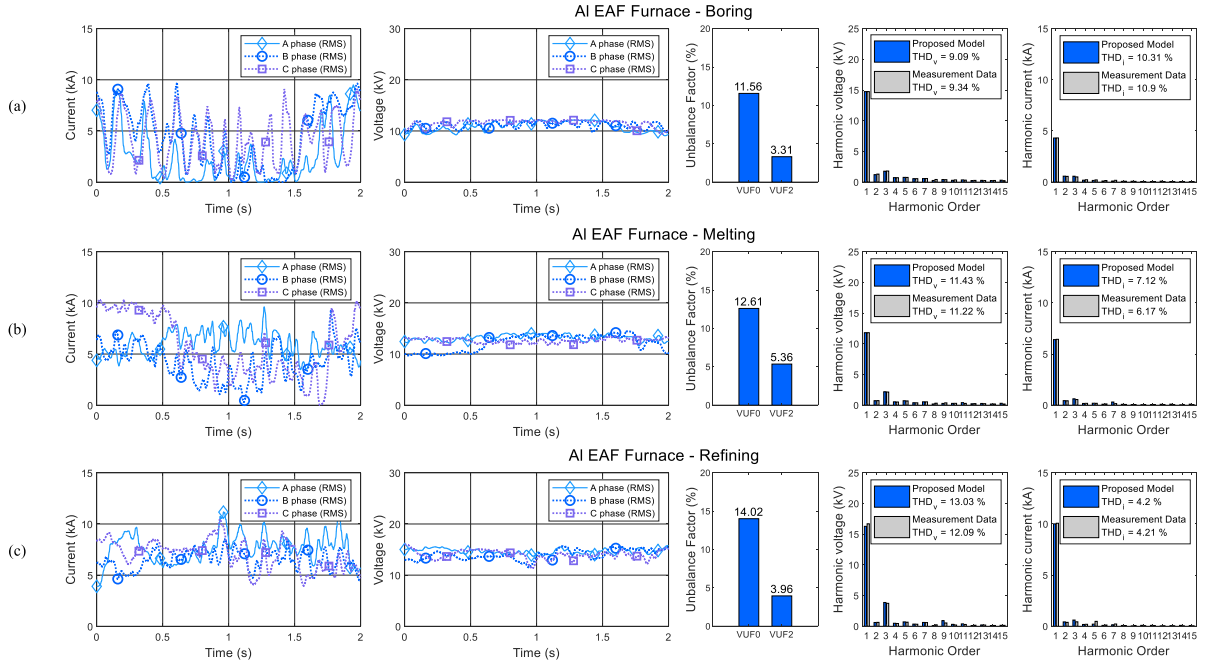

FIGURE 17. Case study result of aluminum furnace system: voltage and current waveform, VUFs, and harmonic spectrum for the three steps: (a) boring, (b) melting, and (c) refining.

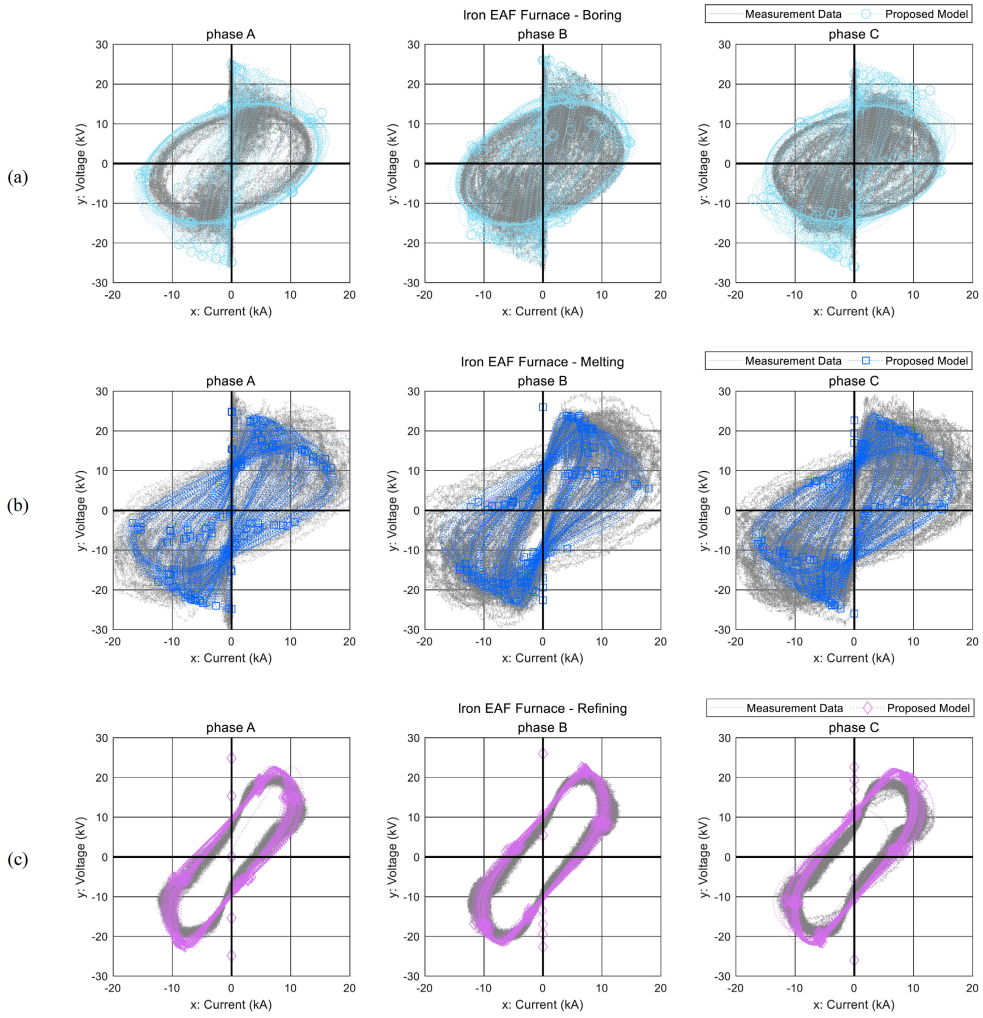

FIGURE 18. Case study result of iron furnace system: comparison of the V–I curve (from measurement data) with the ellipse (from the proposed model) for the three steps: (a) boring, (b) melting, and (c) refining.

follows:

$$\begin{cases} x(t) = \dfrac{V}{\sqrt{R^2 + (\omega L)^2}} \sin(\omega t + \theta_{\mathrm{i}}) \\ y(t) = V \sin(\omega t + \theta_{\mathrm{v}}) \end{cases} \tag{11}$$

Based on these observations, the ellipse corresponding to the EAF system can be formed with both resistance and reactance as shown in Fig. 9. As observed in Fig. 9, the x-intercept is the magnitude of the measured current, I (equal to $V/\sqrt{R^2 + (\omega L)^2}$), and the y-intercept is the magnitude of measured voltage, V, expressed as (8). It is thus confirmed that the impedance components determine the shape of the ellipse representing the EAF system. For instance, the size of the impedance (θ_{ARC} in (4)) determines the tilting angle of the ellipse, as shown in Fig. 9.

The correlation between the impedance components and the V–I characteristics is demonstrated with the actual measurement data. In Section II, Fig. 4 already illustrated that the two ellipses are similar in shape, that is, the model based on the ellipse formula (1) corresponds to the existing EAF system. The ellipse is then illustrated based on the time-varying impedance model in (11), as shown in Fig. 10. In summary, it is verified that the ellipse model, consisting of the time-varying impedance, can appropriately describe the characteristics of the actual EAF system, as shown in Fig. 10.

C. EFFECT OF THE THIRD HARMONIC COMPONENTS AND POWER OSCILLATIONS

Among all the harmonic components in the V–I data for an existing EAF system, the fundamental and the third-harmonic components generally have a dominant magnitude [7]. For instance, the actual measurement data for the iron furnace system are presented in Fig. 11. The central part of the ellipse is concave, owing to the third harmonic component. Based on the information on the harmonic components, the ellipse formula is obtained as follows:

$$\begin{cases} v(t) = V_1 \sin(\omega t + \theta_{\mathrm{v1}}) + V_3 \sin(3\omega t + \theta_{\mathrm{v3}}) \\ i(t) = I_1 \sin(\omega t + \theta_{\mathrm{i1}}) + I_3 \sin(3\omega t + \theta_{\mathrm{i3}}) \end{cases} \tag{12}$$

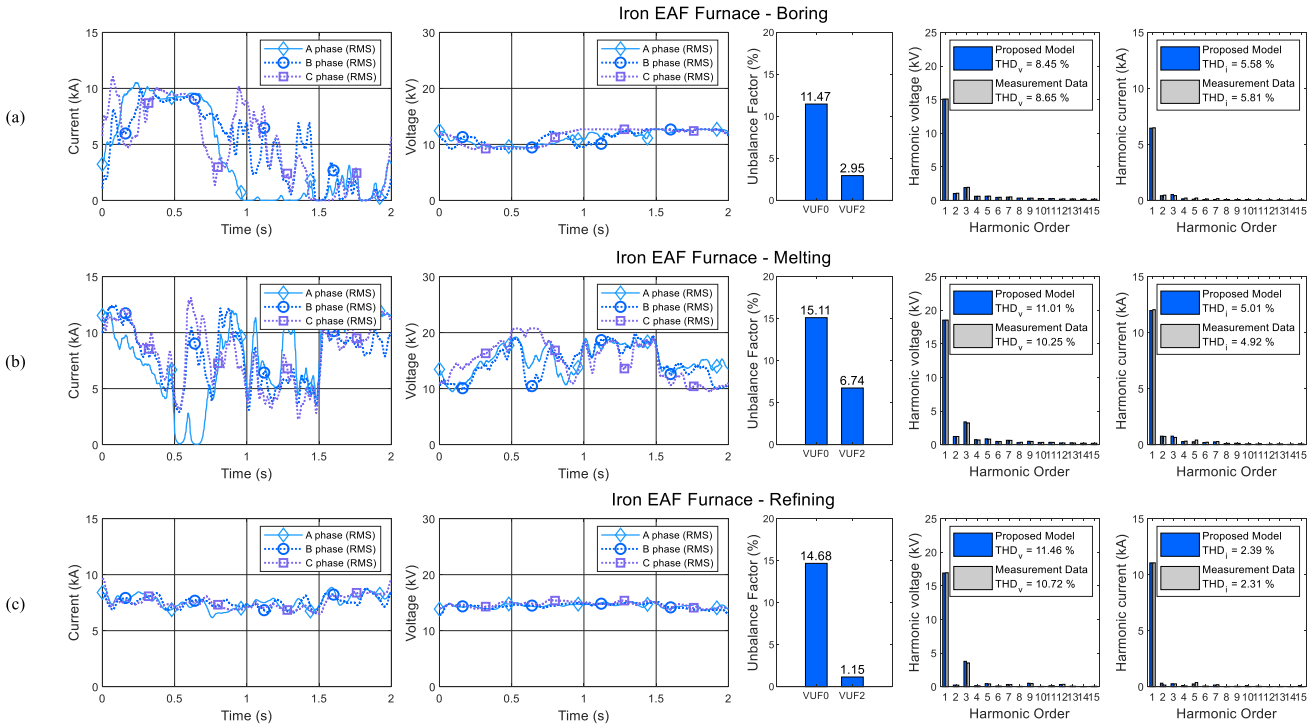

FIGURE 19. Case study result of iron furnace system: voltage and current waveform, VUFs, and harmonic spectrum for the three steps: (a) boring, (b) melting, and (c) refining.

where V_1, θ_{v1}, V_3, θ_{v3}, I_1, θ_{i1}, I_3, and θ_{i3} are the values obtained through the FFT, and $v(t)$ and $i(t)$ are the voltage and current functions based on the measurement data, respectively.

Illustrating the ellipse including the fundamental and the third harmonic component information, the ellipse (gray) determined from the V–I measurement is similar in size and shape to the curve (blue) based on (12) as shown in Fig. 12. This indicates that the third harmonic component can reshape the ellipse formula for the EAF systems.

Meanwhile, the low-frequency oscillation of the power waveform can also affect the size of the ellipse. Figure 13(b) shows the low-frequency oscillations of the active and reactive power waveforms. The overall size and tilting angle of the ellipse is observed to be consistently fluctuating due to the low-frequency oscillations, as shown in Fig. 13(a).

Considering the relationship in (7), the oscillation of power affects the magnitude of the voltage and current, as it changes $R_{ARC}(t)$ and $L_{ARC}(t)$. A time-varying impedance model is developed in this study which includes the active and reactive power components as shown in (7).

In summary, the developed model can include the effects of harmonics and low-frequency oscillations of the EAF system.

D. MODELING METHOD WITHOUT V–I MEASUREMENT DATA

This section considers the case in which the voltage and current profiles are not given. The system planner often attempts to create an electrical EAF model before constructing the furnace. This study presents an appropriate modeling method for the creation of a pre-study model for the EAF without the field measurement data.

The low-frequency power oscillation and the third harmonic component determine the overall shape of the ellipse model, as explained in the previous section. Thus, these data are required to perform the modeling of the EAF system in advance. Consequently, the generalized data for low-frequency power and harmonics are presented in this study, which can be referenced in the modeling without the field measurement data, particularly for the pre-study in the planning stage.

The modeling process without the V–I profile is demonstrated using the data provided in Tables 1, 2 and 3 (in the Appendix). The overall process is illustrated in Fig. 14.

In contrast to the process starting from (3) in Section III-A, this proposed method acquires the voltage and current information from the data provided in this paper.

$$\begin{cases} v_{m,h}(t) = \sum_{h=1}^{15} \sqrt{2} V_{m,h}(t) \sin(h\omega t + \theta_{v,h}(t)) \\ i_{m,h}(t) = \sum_{h=1}^{15} \sqrt{2} I_{m,h}(t) \sin(h\omega t + \theta_{i,h}(t)) \end{cases} \tag{13}$$

where $V_{m,h}$, $I_{m,h}$, $\theta_{v,h}$ and $\theta_{i,h}$ are the values obtained from the V–I profile in Table 2.

Firstly, the calculations for the active and reactive power components are performed based on (14) and (15),

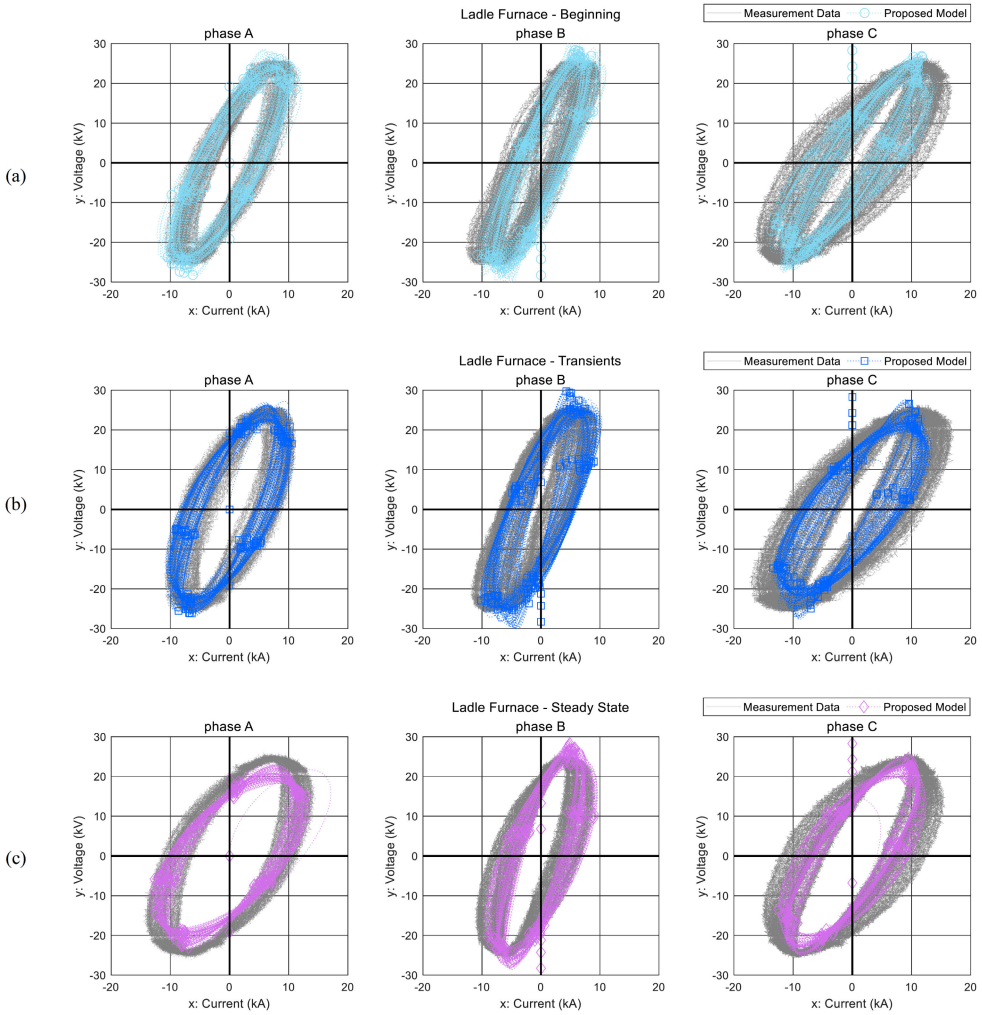

FIGURE 20. Case study result of ladle furnace: comparison of the V–I curve (by measurement data) with the ellipse (from the proposed model) for the three steps: (a) beginning, (b) transients, and (c) steady state.

similar to (5).

$$P_{\text{exam}}(t) = \sum_{h=0.1}^{15} P_{\text{m,h}} \sin(2\pi ht + \theta_{\text{rand}}) \tag{14}$$

$$Q_{\text{exam}}(t) = \sum_{h=0.1}^{15} Q_{\text{m,h}} \sin(2\pi ht + \theta_{\text{rand}}) \tag{15}$$

where θ_{rand} is the random angle value, and $P_{\text{m,h}}$ and $Q_{\text{m,h}}$ are the active and reactive power values for the low-frequency components (from 0.1 Hz to 15 Hz in this paper), respectively.

These power components include the low-frequency information in Table 3 since the low-frequency power is a major factor in the determination of the V–I characteristics of the EAF as shown in Fig. 13.

Based on (14) and (15), the power calculations are performed for the EAF system. Using the generalized data in Table 1, the power rating (P_{rated} and Q_{rated}) and the average power values, (P_{avg} and Q_{avg}) can be proportionally adjusted corresponding to the rating of the target system. The values can then be practically scaled depending on the system, as follows:

$$P_{\text{DAT}}(t) = \frac{(P_{\text{exam}}(t) + P_{\text{avg}})P_{\text{rated}}}{P_{\text{base}}} \tag{16}$$

$$Q_{\text{DAT}}(t) = \frac{(Q_{\text{exam}}(t) + Q_{\text{avg}})Q_{\text{rated}}}{Q_{\text{base}}} \tag{17}$$

As the current function in (13), the RMS current component is obtained as follows:

$$I_{\text{DAT}}(t) = \frac{1}{\sqrt{2}} \sqrt{\sum_{h=1}^{15} i_{\text{m,h}}^2(t)} \tag{18}$$

Similar to (7), the time-varying impedance components are obtained as follows:

$$R_{\text{ARC}}(t) = \frac{P_{\text{DAT}}(t)}{I_{\text{DAT}}^2(t)} \tag{19}$$

$$L_{\text{ARC}}(t) = \frac{Q_{\text{DAT}}(t)}{\omega I_{\text{DAT}}^2(t)} \tag{20}$$

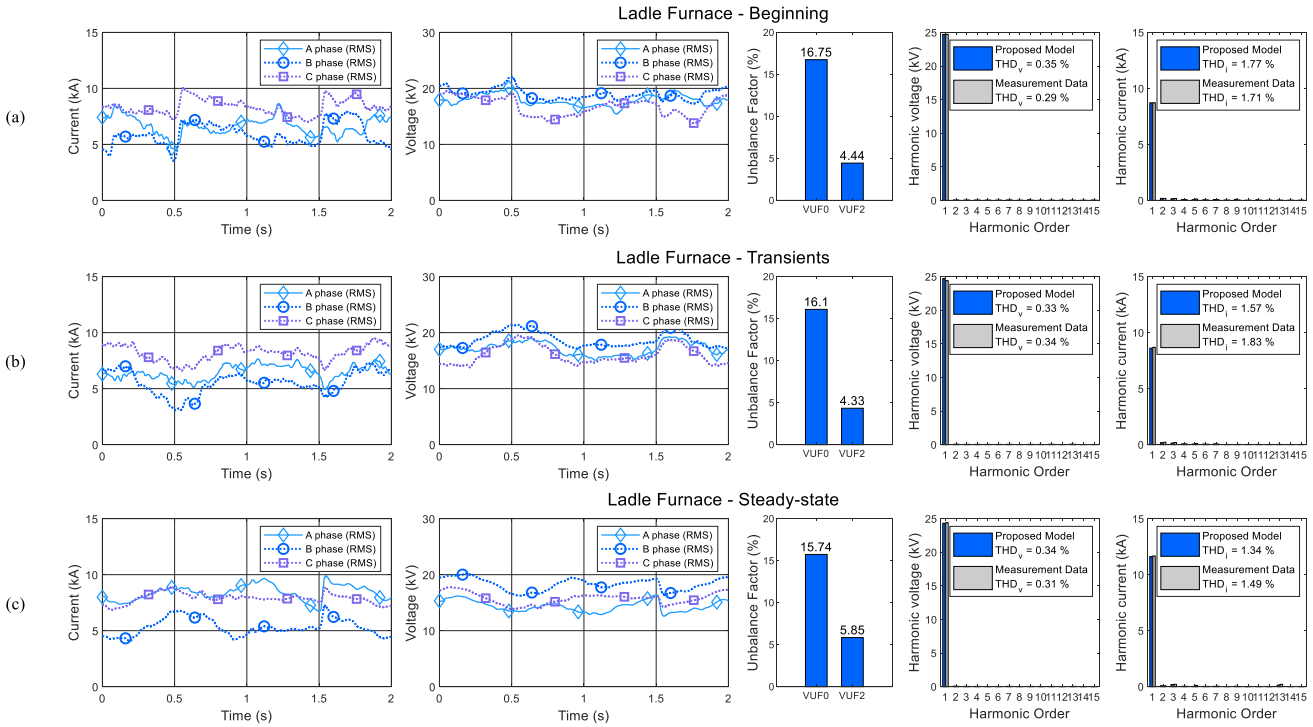

FIGURE 21. Case study result of ladle furnace system: voltage and current waveform, VUFs, and harmonic spectrum for the three steps: (a) beginning, (b) transients, and (c) steady state.

To demonstrate the modeling process, the ellipse with (14)–(20) based on the generalized data is presented in Fig. 15. It is observed that the method accurately describes the V–I characteristics of the EAF system. Most importantly, this method enables system engineers to model and assess the EAF system at the planning stage without the V–I profiles.

IV. CASE STUDY

A. ALUMINUM FURNACE SYSTEM

This section demonstrates the applications of the proposed modeling method for an aluminum furnace system. A time-varying impedance model is formulated in the PSCAD/EMTDC simulation based on the V–I field data of the aluminum furnace. As described in Section III, the ellipse formulae are based on the process illustrated in Fig. 5. A model is developed corresponding to each of the three processes of aluminum smelting, i.e., boring, melting, and refining. The results of the case study are presented in Fig. 16. The ellipses (gray) drawn by the V–I measurement data and the curves (cyan, blue, and purple) drawn through the simulation are identical in size and shape.

Additionally, the voltage and current waveforms in the time-domain for the V–I curve of Fig. 16 are presented in Fig. 17. As shown in Fig. 17, the fluctuation of the current waveform has a random characteristic. To assess the unbalance condition for the proposed model of EAF system, the voltage unbalance factors (VUF) are defined by classified into the zero sequence (VUF_0) and the negative sequence (VUF_2) [40].

$$VUF_0 = \frac{V_0}{V_1} \cdot 100[\%] \tag{21}$$

$$VUF_2 = \frac{V_2}{V_1} \cdot 100[\%] \tag{22}$$

where V_0, V_1, and V_2 are the zero, positive and negative sequence component of voltage, respectively.

The voltage unbalance factors (VUF_0 and VUF_2) according to (21) and (22) are also analyzed in Fig. 17. In the comparison of FFT results of voltage and current, it is confirmed that the harmonic spectrum in the proposed model matches the spectrum in the measurement profile. To compare the total harmonic distortion (THD) values of the measurement profile with the values of the proposed model, the THD values for voltage (THD_v) and for current (THD_i) in the measurement profiles are similar to the THD values of the proposed model within an error of 0.7 %. This indicates that the proposed impedance model contains the V–I characteristics of the aluminum furnace system.

B. IRON FURNACE SYSTEM

The application of the proposed modeling method to an iron furnace system is demonstrated in this case study. The shape of the ellipse is remarkably distorted as it causes severe harmonics, especially the third harmonic component as shown in Fig. 18. Nevertheless, it is verified that the proposed method can include nonlinear features as shown in Fig. 18. The ellipses (gray) drawn by the V–I measurement data and the

TABLE 1. Rating and average power for each case.

		Average	Rating
Case 1 (EAF Iron Boring)	P (MW)	65.132	100
	Q (Mvar)	76.156	100
Case 2 (EAF Iron Melting)	P	201	250
	Q	151	250
Case 3 (EAF Iron Refining)	P	189	200
	Q	120	150
Case 4 (EAF Aluminum Boring)	P	62	120
	Q	45	120
Case 5 (EAF Aluminum Melting)	P	72	120
	Q	51	100
Case 6 (EAF Aluminum Refining)	P	173	250
	Q	102	200
Case 7 (Ladle Beginning)	P	172	200
	Q	105	150
Case 8 (Ladle Transients)	P	144	200
	Q	133	200
Case 9 (Ladle Steady state)	P	146	250
	Q	176	200

curves (cyan, blue, and purple) drawn through the simulation are identical in size and shape.

Moreover, the voltage and current waveforms in the time-domain for the V–I curve of Fig. 18 are analyzed in Fig. 19. The fluctuations of the waveforms of the current and voltage has a quite nonlinear characteristic as shown in Fig. 19. As discussed in Section 1, in the refining stage, the current and voltage magnitude exhibit the least amount of change compared to the two previous stages. The voltage unbalance factors according to (21) and (22) are also provided in Fig. 19. In the comparison of FFT results of voltage and current, it is confirmed that the harmonic spectrum in the proposed model matches the spectrum in the measurement profile. Also, THD_{v} and THD_{i} in the proposed model are similar to the THD values in the measurement profile within an error of 0.76 %. This demonstrates that the proposed impedance model contains the V–I characteristics of the iron furnace system.

C. LADLE FURNACE SYSTEM

The case study of the LF system demonstrates the application of the proposed modeling method. The time-varying impedance model is formulated in the case study using the V–I measurement data of the real LF system. A model is developed corresponding to each of the three processes for a ladle melt furnace: beginning, transient, and steady state. The results of the case study are analyzed in Fig. 20. The ellipses (gray) drawn by the V–I measurement data and the curves (cyan, blue, and purple) drawn through the simulation are identical in size and shape.

In addition, the voltage and current waveforms in the time-domain for the V–I curve of Fig. 20 are analyzed in Fig. 21. As shown in Fig. 21, the fluctuation of the current waveform has a random characteristic. The values for the voltage unbalance factors according to (21) and (22) are also presented in Fig. 21. Compared to the aluminum furnace and iron furnace, the overall harmonic component is relatively small, and therefore THD_{v} and THD_{i} also have lower values as shown in Fig. 21. In the comparison of FFT results of voltage and current, it is confirmed that the harmonic spectrum in the proposed model matches the spectrum in the measurement profile. THD_{v} and THD_{i} in the proposed model are also similar to the values in the measurement profile within an error of 0.34 %. This verifies that the proposed impedance model includes the V–I characteristics of the real LF system.

TABLE 2. Main harmonics information for EAFs.

		1st	2nd	3rd	4th	5th	6th	7th	8th	9th	10th	11th	12th	13th	14th	15th
Case 1	V mag (kV)	15.084	1.068	1.946	0.624	0.643	0.468	0.522	0.349	0.340	0.287	0.279	0.236	0.218	0.199	0.187
	V phase (rad)	1.530	-0.005	-0.430	-0.288	0.275	-0.058	0.163	0.906	0.712	0.866	0.246	0.542	0.952	-0.406	-0.265
	I mag (kA)	6.483	0.470	0.427	0.211	0.213	0.131	0.159	0.075	0.070	0.059	0.053	0.047	0.043	0.040	0.036
	I phase (rad)	0.796	0.154	-0.565	0.275	0.614	-0.003	-0.254	0.161	-0.586	0.942	-0.247	0.825	-0.602	-0.163	-0.216
Case 2	V mag	18.534	1.214	3.225	0.692	0.814	0.455	0.633	0.115	0.112	0.084	0.083	0.066	0.063	0.054	0.051
	V phase	0.855	0.324	1.008	0.060	0.309	0.081	-0.357	-0.191	0.785	-0.088	0.269	-0.693	0.078	-0.365	0.405
	I mag	12.047	0.734	0.646	0.311	0.408	0.215	0.271	0.115	0.112	0.084	0.083	0.066	0.063	0.054	0.051
	I phase	0.239	-0.036	0.057	-0.101	-0.249	0.130	-0.032	0.457	0.019	0.931	-0.652	-0.859	0.859	1.007	0.858
Case 3	V mag	16.954	0.221	3.529	0.123	0.410	0.089	0.305	0.050	0.464	0.044	0.137	0.035	0.066	0.029	0.066
	V phase	0.856	-0.120	0.752	0.143	1.298	-0.164	1.475	0.710	-0.653	0.530	-0.208	0.770	-0.875	0.877	0.807
	I mag	11.055	0.143	0.248	0.065	0.364	0.046	0.172	0.022	0.026	0.019	0.033	0.015	0.020	0.013	0.015
	I phase	0.271	0.437	-1.181	-0.026	0.199	0.161	-1.649	0.524	-0.271	-0.499	-0.136	0.389	0.993	0.101	0.896
Case 4	V mag	14.744	1.307	1.807	0.718	0.766	0.558	0.577	0.430	0.394	0.358	0.323	0.279	0.259	0.266	0.233
	V phase	0.924	0.034	1.489	0.319	-0.157	-0.075	-0.002	0.273	-0.606	-0.216	-0.490	-0.422	-0.243	-0.426	-0.141
	I mag	4.317	0.562	0.511	0.230	0.216	0.150	0.175	0.085	0.073	0.062	0.056	0.050	0.046	0.042	0.040
	I phase	0.330	0.248	-0.136	0.040	-0.569	-0.109	0.150	-0.571	0.022	-0.008	0.061	0.424	0.437	-0.630	0.948
Case 5	V mag	11.811	0.743	2.146	0.521	0.698	0.388	0.543	0.328	0.382	0.302	0.296	0.253	0.247	0.201	0.193
	V phase	0.652	-0.003	0.938	-0.290	0.103	0.107	-0.069	0.288	-0.578	0.144	-0.633	0.729	0.453	-0.223	0.711
	I mag	6.439	0.433	0.551	0.181	0.185	0.126	0.155	0.075	0.067	0.057	0.053	0.043	0.041	0.038	0.034
	I phase	0.036	-0.099	0.576	0.385	0.453	-0.274	-0.311	0.323	-0.629	-0.374	0.169	-0.286	-0.356	-0.022	0.445
Case 6	V mag	16.706	0.641	3.741	0.458	0.670	0.338	0.604	0.241	0.548	0.212	0.300	0.173	0.208	0.135	0.154
	V phase	0.525	-0.255	0.265	-0.254	0.143	0.042	0.183	-0.844	-0.842	0.156	-0.430	-0.160	-0.099	-0.380	0.545
	I mag	10.072	0.387	0.439	0.195	0.483	0.127	0.224	0.067	0.080	0.049	0.057	0.039	0.040	0.032	0.032
	I phase	-0.002	0.083	0.042	0.036	1.283	-0.036	0.448	-0.750	0.653	-0.265	-0.182	-0.127	0.929	-0.794	0.771
Case 7	V mag	24.718	0.055	0.048	0.046	0.044	0.039	0.066	0.022	0.043	0.025	0.046	0.021	0.057	0.022	0.027
	V phase	0.889	0.502	-0.195	1.202	-0.904	0.146	-0.106	0.555	0.201	-0.113	0.412	0.648	0.186	-0.501	0.059
	I mag	8.720	0.179	0.169	0.058	0.122	0.041	0.059	0.024	0.030	0.019	0.021	0.017	0.017	0.016	0.016
	I phase	0.347	0.224	0.409	-0.133	-0.821	0.087	-0.639	0.911	0.777	0.697	1.002	-0.006	0.137	-0.294	0.383
Case 8	V mag	24.397	0.066	0.048	0.047	0.039	0.037	0.053	0.022	0.043	0.025	0.046	0.021	0.057	0.022	0.027
	V phase	0.924	0.034	1.489	0.319	-0.157	-0.075	-0.002	0.273	-0.606	-0.216	-0.490	-0.422	-0.243	-0.426	-0.141
	I mag	8.689	0.210	0.063	0.096	0.043	0.057	0.018	0.023	0.017	0.017	0.017	0.016	0.016	0.014	0.016
	I phase	0.160	0.085	0.669	0.137	0.495	0.131	0.371	0.074	0.373	-0.527	0.772	0.958	0.735	-0.322	0.603
Case 9	V mag	24.401	0.059	0.043	0.040	0.028	0.024	0.044	0.023	0.044	0.025	0.043	0.020	0.053	0.022	0.029
	V phase	1.176	0.307	0.058	0.077	-0.118	0.497	1.312	-0.510	0.135	-0.077	0.019	-0.051	-0.505	0.159	-0.144
	I mag	11.667	0.082	0.208	0.039	0.115	0.028	0.051	0.016	0.020	0.018	0.017	0.014	0.207	0.014	0.013
	I phase	0.307	0.760	1.031	-0.907	-0.022	-0.004	-1.116	-0.808	-0.481	-0.573	0.913	0.575	-0.648	0.285	0.842

V. CONCLUSION

This paper presents a methodology for modeling the EAF systems using the V–I profile, which is verified through case studies using the measurement data of the existing EAFs. The measurement-based model includes the realistic characteristics of the EAF system for three processes: boring, melting, and refining. A detailed EAF model is established by associating with the ellipse formula, which includes the effects of the power oscillations and the harmonic components. Furthermore, this study introduces the concept of

TABLE 3. Real field data of industry EAF for low-frequency power.

	Case 1		Case 2		Case 3		Case 4		Case 5		Case 6		Case 7		Case 8		Case 9	
Freq.	P (MW)	Q (Mvar)	P	Q	P	Q	P	Q	P	Q	P	Q	P	Q	P	Q	P	Q
0.1 Hz	0.0099	0.0000	0.0173	0.0000	0.0091	0.0129	0.0020	0.0000	0.0039	0.0000	0.0321	0.0000	0.0398	0.0000	0.0263	0.0000	0.0085	0.0000
0.2 Hz	0.0179	0.0001	0.0233	0.0000	0.0298	0.0389	0.0075	0.0000	0.0259	0.0000	21.2242	0.1941	0.0176	0.0000	0.0119	0.0000	0.0361	0.0000
0.3 Hz	0.0176	0.0001	0.0642	0.0000	0.0261	0.0364	0.0058	0.0000	0.0084	0.0000	0.0275	0.0000	0.0096	0.0000	0.0066	0.0000	0.0412	0.0000
0.4 Hz	0.0393	0.0000	0.0197	0.0000	0.0092	0.0136	0.0023	0.0000	0.0037	0.0000	31.7555	2.2930	0.0105	0.0000	0.0441	0.0000	0.0135	0.0000
0.5 Hz	61.1461	25.3434	64.2004	10.1769	5.5458	8.9197	44.3304	5.9907	26.8264	1.0490	0.0325	0.0000	9.9185	1.3647	23.0652	2.0358	13.0346	0.7503
0.6 Hz	0.0243	0.0001	0.0529	0.0000	0.0073	0.0152	0.0033	0.0000	0.0021	0.0000	10.3690	0.2483	0.0283	0.0000	0.0326	0.0000	0.0373	0.0000
0.7 Hz	0.0254	0.0002	0.0218	0.0000	0.0796	0.0442	0.0352	0.0001	0.0047	0.0000	0.0214	0.0000	0.0404	0.0000	0.0272	0.0000	0.0677	0.0000
0.8 Hz	0.0111	0.0001	0.0073	0.0000	0.0192	0.0421	0.0173	0.0001	0.0151	0.0000	4.7305	0.0645	0.0598	0.0000	0.0318	0.0000	0.0449	0.0000
0.9 Hz	0.0337	0.0001	0.0391	0.0000	0.0074	0.0152	0.0022	0.0000	0.0030	0.0000	0.0186	0.0000	0.0200	0.0000	0.0288	0.0000	0.0348	0.0000
1 Hz	12.0285	2.8339	49.6270	7.4688	6.9080	7.3415	11.6718	0.6941	12.1878	0.1553	7.1046	0.1598	18.6217	1.5565	41.5422	7.3769	30.4834	1.7532
2 Hz	10.5052	0.4706	21.6555	0.5383	4.7242	4.6455	5.8276	0.2655	8.3903	0.1043	12.1077	0.1111	18.9685	0.5792	14.6567	1.1047	13.0911	0.1506
3 Hz	6.4202	0.1667	8.2658	0.7107	3.3285	4.3350	1.2219	0.0398	3.5613	0.0285	3.3543	0.0740	6.2885	0.1700	3.9929	0.0377	1.4610	0.0226
4 Hz	4.3327	0.1399	27.4451	0.1116	3.1101	4.0930	4.5043	0.2538	3.2609	0.0366	2.4211	0.0300	2.3820	0.0765	3.2296	0.1128	4.9107	0.0240
5 Hz	7.8836	0.3692	12.9550	0.4879	1.1951	1.8724	11.6804	0.7321	1.5014	0.0226	4.6329	0.0666	4.1216	0.0599	1.1156	0.0227	2.7322	0.0135
6 Hz	5.1491	0.0298	6.5390	0.3235	2.1865	1.2966	1.0602	0.0301	5.6771	0.0645	3.5695	0.0251	5.5787	0.0495	1.0388	0.0040	2.4469	0.0254
7 Hz	4.4995	0.0629	5.0767	0.1272	1.5944	1.9126	6.6993	0.2949	3.5740	0.0773	7.4763	0.1199	2.4805	0.0203	2.4312	0.0455	3.6019	0.0237
8 Hz	5.0633	0.0950	7.3137	0.1263	1.1177	1.7317	3.2300	0.1498	2.6682	0.0189	4.5622	0.0486	1.8579	0.0101	1.1716	0.0141	1.6910	0.0111
9 Hz	1.8536	0.0936	4.8550	0.1386	0.6757	1.5394	7.7606	0.1947	2.2997	0.0130	2.8609	0.0378	4.6222	0.0464	0.8892	0.0070	1.9352	0.0104
10 Hz	2.8504	0.0823	1.4621	0.0316	0.7109	1.3312	3.3916	0.0800	6.8740	0.0698	2.2620	0.0093	1.0725	0.0051	0.7509	0.0022	1.1852	0.0035
11 Hz	3.9615	0.1002	5.7141	0.1542	0.8593	1.4174	3.8863	0.0634	2.6757	0.0202	0.6108	0.0017	0.8410	0.0062	1.0074	0.0113	0.9262	0.0010
12 Hz	2.3020	0.0871	8.3608	0.1343	0.8169	0.9504	1.8067	0.0332	2.7027	0.0313	2.0064	0.0072	0.8056	0.0056	0.9495	0.0031	1.5119	0.0032
13 Hz	5.5346	0.1400	4.8921	0.1139	0.7588	0.9836	0.0668	0.0004	1.1343	0.0122	1.5309	0.0080	1.0474	0.0036	1.3549	0.0077	1.1455	0.0028
14 Hz	0.2205	0.0047	4.1400	0.0371	0.8470	1.1625	1.4405	0.0296	2.4748	0.0214	3.8061	0.0140	0.4231	0.0009	0.1450	0.0019	1.4444	0.0074
15 Hz	3.6511	0.0637	2.6918	0.0731	0.9493	1.2355	2.6725	0.0668	3.9280	0.0106	2.8190	0.0116	1.3464	0.0077	0.6149	0.0018	0.9160	0.0035

generating an EAF model without the V–I measurement data. Based on the data presented in this paper, the EAF model can be formulated at the planning stage using the proposed method. The proposed model is observed to accurately present the detailed characteristics of the EAF system, as demonstrated through the realistic case studies. Therefore, the findings of this research significantly contribute to the development of EAF systems and help in modeling and analyzing EAF systems.

APPENDIX. GENERALIZED DATA FOR EAF MODELING

The generalized data used to formulate an EAF model without the field measurements are listed in Tables 1, 2, and 3.

REFERENCES

[1] I. Vervenne, K. Van Reusel, and R. Belmans, "Electric arc furnace modelling from a 'power quality' point of view," in *Proc. 9th Int. Conf. Elect. Power Quality Utilisation*, Oct. 2007, pp. 1–6.

[2] Y. Varetsky, V. Konoval, and Z. Hanzelka, "A method of evaluating FACTS device impact on voltage flicker in the EAF supply system," in *Proc. 12th Int. Conf. Exhib. Electr. Power Quality Utilisation (EPQU)*, Sep. 2020, pp. 1–4.

[3] M. Gala, A. Sawicki, and K. Jagiela, "Modeling of asymmetrical operating states of AC electric arc furnace in the power system," in *Proc. Appl. Electromagn. Modern Eng. Med. (PTZE)*, Jun. 2019, pp. 42–46.

[4] O. Salor, B. Gultekin, S. Buhan, B. Boyrazoglu, T. Inan, T. Atalik, A. Acik, A. Terciyanli, O. Unsar, E. Altintas, Y. Akkaya, E. Ozdemirci, I. Cadirci, and M. Ermis, "Electrical power quality of iron and steel industry in Turkey," *IEEE Trans. Ind. Appl.*, vol. 46, no. 1, pp. 60–80, Jan. 2010.

[5] L. F. Beites, J. G. Mayordomo, A. Hernandez, and R. Asensi, "Harmonics, interharmonics and unbalances of arc furnaces: A new frequency domain approach," *IEEE Trans. Power Del.*, vol. 16, no. 4, pp. 661–668, Oct. 2001.

[6] I. R. Abdulveleev, T. R. Khramshin, G. P. Kornilov, and R. R. Abdulveleeva, "Experimental study of the impact of a DC electric arc furnace on a power grid," in *Proc. Int. Conf. Ind. Eng., Appl. Manuf. (ICIEAM)*, May 2021, pp. 214–218.

[7] D. Andrews, M. T. Bishop, and J. F. Witte, "Harmonic measurements, analysis, and power factor correction in a modern steel manufacturing facility," *IEEE Trans. Ind. Appl.*, vol. 32, no. 3, pp. 617–624, May 1996.

[8] B. Boulet, G. Lalli, and M. Ajersch, "Modeling and control of an electric arc furnace," in *Proc. Amer. Control Conf.*, Jun. 2003, pp. 3060–3064.

[9] G. C. Montanari, M. Loggini, L. Pitti, E. Tironi, and D. Zaninelli, "The effects of series inductors for flicker reduction in electric power systems supplying arc furnaces," in *Proc. Conf. Rec. IEEE Ind. Appl. Conf. 28th IAS Annu. Meeting*, Oct. 1993, pp. 1496–1503.

[10] C. Ö. Gerçek, M. Ermis, A. Ertas, K. N. Kose, and Ö. Ünsar, "Design, implementation, and operation of a new C-type 2nd harmonic filter for electric arc and ladle furnaces," *IEEE Trans. Ind. Appl.*, vol. 47, no. 4, pp. 1545–1557, Jul. 2011.

[11] E. Balouji, O. Salor, and M. Ermis, "Exponential smoothing of multiple reference frame components with GPUs for real-time detection of time-varying harmonics and interharmonics of EAF currents," *IEEE Trans. Ind. Appl.*, vol. 54, no. 6, pp. 6566–6575, Nov. 2018.

[12] E. Uz-Logoglu, O. Salor, and M. Ermis, "Real-time detection of interharmonics and harmonics of AC electric arc furnaces on GPU framework," *IEEE Trans. Ind. Appl.*, vol. 55, no. 6, pp. 6613–6623, Nov. 2019.

[13] Y. E. Vatankulu, Z. Senturk, and O. Salor, "Harmonics and interharmonics analysis of electrical arc furnaces based on spectral model optimization with high-resolution windowing," *IEEE Trans. Ind. Appl.*, vol. 53, no. 3, pp. 2587–2595, May 2017.

[14] S. Morello, T. J. Dionise, and T. L. Mank, "Comprehensive analysis to specify a static var compensator for an electric arc furnace upgrade," *IEEE Trans. Ind. Appl.*, vol. 51, no. 6, pp. 4840–4852, Nov. 2015.

[15] F. Shojaei, H. Samet, and T. Ghanbari, "Electric arc furnaces reactive power optimized calculation used in SVC," *IEEE Trans. Ind. Electron.*, early access, Jun. 16, 2021, doi: 10.1109/TIE.2021.3088373.

[16] A. Kavousi-Fard, W. Su, T. Jin, A. S. Al-Sumaiti, H. Samet, and A. Khosravi, "A predictive KH-based model to enhance the performance of industrial electric arc furnaces," *IEEE Trans. Ind. Electron.*, vol. 66, no. 10, pp. 7976–7985, Oct. 2019.

[17] A. A. Nikolaev and P. G. Tulupov, "Electric arc furnace control system with smelting stage diagnostic function and adaptive non-linear impedance controller," in *Proc. Int. Conf. Ind. Eng., Appl. Manuf. (ICIEAM)*, May 2021, pp. 581–585.
[18] A. A. Nikolaev, P. G. Tulupov, and V. S. Ivekeev, "Comparative analysis of modern electric control systems of electric arc furnaces," in *Proc. Int. Ural Conf. Electr. Power Eng. (UralCon)*, Sep. 2020, pp. 464–468.
[19] T. Lu, Y. Sun, P. Shen, P. An, and S. Diao, "Study on time-varying resistance model of arc furnace based on arc length modulation and PSO algorithm," in *Proc. IEEE/IAS Ind. Commercial Power Syst. Asia (I&CPS Asia)*, Jul. 2020, pp. 513–518.
[20] E. Altıntaş, Ö. Salor, I. Çadırcı, and M. Ermiş, "A new flicker contribution tracing method based on individual reactive current components of multiple EAFs at PCC," *IEEE Trans. Ind. Appl.*, vol. 46, no. 5, pp. 1746–1754, Sep. 2010.
[21] C.-I. Chen and Y.-C. Chen, "A neural-network-based data-driven nonlinear model on time- and frequency-domain voltage–current characterization for power-quality study," *IEEE Trans. Power Del.*, vol. 30, no. 3, pp. 1577–1584, Jun. 2015.
[22] M. T. Esfahani and B. Vahidi, "A new stochastic model of electric arc furnace based on hidden Markov model: A study of its effects on the power system," *IEEE Trans. Power Del.*, vol. 27, no. 4, pp. 1893–1901, Oct. 2012.
[23] G. W. Chang, M.-F. Shih, Y.-Y. Chen, and Y.-J. Liang, "A hybrid wavelet transform and neural-network-based approach for modelling dynamic voltage-current characteristics of electric arc furnace," *IEEE Trans. Power Del.*, vol. 29, no. 2, pp. 815–824, Apr. 2014.
[24] H. Mokhtari and M. Hejri, "A new three phase time-domain model for electric arc furnaces using MATLAB," in *Proc. IEEE/PES Transmiss. Distrib. Conf. Exhib.*, Oct. 2002, pp. 2078–2083.
[25] A. Bracale, P. Caramia, G. Carpinelli, P. De Falco, and A. Russo, "Comparison of DC electric arc furnace chaotic models for power quality indices assessment," *IEEE Trans. Ind. Appl.*, early access, Aug. 20, 2021, doi: 10.1109/TIA.2021.3106569.
[26] E. Uz-Logoglu, O. Salor, and M. Ermis, "Online characterization of interharmonics and harmonics of AC electric arc furnaces by multiple synchronous reference frame analysis," *IEEE Trans. Ind. Appl.*, vol. 52, no. 3, pp. 2673–2683, May 2016.
[27] E. Sezgin and O. Salor, "Analysis of power system harmonic subgroups of the electric arc furnace currents based on a hybrid time-frequency analysis method," *IEEE Trans. Ind. Appl.*, vol. 55, no. 4, pp. 4398–4406, Jul. 2019.
[28] N. Severoglu and O. Salor, "Statistical models of EAF harmonics developed for harmonic estimation directly from waveform samples using deep learning framework," *IEEE Trans. Ind. Appl.*, early access, Sep. 21, 2021, doi: 10.1109/TIA.2021.3114127.
[29] E. Balouji, K. Backstrom, T. McKelvey, and O. Salor, "Deep-learning-based harmonics and interharmonics predetection designed for compensating significantly time-varying EAF currents," *IEEE Trans. Ind. Appl.*, vol. 56, no. 3, pp. 3250–3260, May 2020.
[30] A. Kavousi-Fard, A. Khosravi, and S. Nahavandi, "Reactive power compensation in electric arc furnaces using prediction intervals," *IEEE Trans. Ind. Electron.*, vol. 64, no. 7, pp. 5295–5304, Jul. 2017.
[31] F. Martell-Chavez, M. E. Macias-Garcia, and A. R. Izaguirre-Alegria, "Performance parameters of electric arc furnaces based on the current's physical components power theory," *IEEE Trans. Ind. Appl.*, vol. 56, no. 6, pp. 6076–6082, Nov. 2020.
[32] R. Horton, T. A. Haskew, and R. F. Burch IV, "A time-domain AC electric arc furnace model for flicker planning studies," *IEEE Trans. Power Del.*, vol. 24, no. 3, pp. 1450–1457, Jul. 2009.
[33] M. Gol, O. Salor, B. Alboyaci, B. Mutluer, I. Cadirci, and M. Ermis, "A new field-data-based EAF model for power quality studies," *IEEE Trans. Ind. Appl.*, vol. 46, no. 3, pp. 1230–1242, May 2010.
[34] F. Illahi, I. El-Amin, and M. U. Mukhtiar, "The application of multiobjective optimization technique to the estimation of electric arc furnace parameters," *IEEE Trans. Power Del.*, vol. 33, no. 4, pp. 1727–1734, Aug. 2018.
[35] A. T. Teklić, B. Filipović-Grčić, and I. Pavić, "Modelling of three-phase electric arc furnace for estimation of voltage flicker in power transmission network," *Electr. Power Syst. Res.*, vol. 146, pp. 218–227, May 2017.
[36] L. Hocine, D. Yacine, B. Kamel, and K. M. Samira, "Improvement of electrical arc furnace operation with an appropriate model," *Energy*, vol. 34, no. 9, pp. 1207–1214, Sep. 2009.
[37] Z. Ping, Z. Tao, and X. Chenjing, "Modeling of ac arc furnace and its influence on the relay protection," in *Proc. CICED*, 2010, pp. 1–6.
[38] A. Wolf and M. Thamodharan, "Reactive power reduction in three-phase electric arc furnace," *IEEE Trans. Ind. Electron.*, vol. 47, no. 4, pp. 729–733, Aug. 2000.
[39] E. A. Cano-Plata, A. J. U. Farfan, and O. J. S. Marin, "Electric arc furnace model in distribution systems," *IEEE Trans. Ind. Appl.*, vol. 51, no. 5, pp. 4313–4320, Sep. 2015.
[40] R. C. Dugan, M. F. McGranaghan, S. Surya, and B. H. Wayne, *Electrical Power Systems Quality*, 2nd ed. New York, NY, USA: McGraw-Hill, 2003.

CHOONGMAN LEE (Member, IEEE) received the Ph.D. degree in electrical engineering from Yonsei University, Seoul, South Korea. He is currently a Researcher at Korea Railroad Research Institute, South Korea. His research interests include modeling and control of power converters, power electronic applications in power systems, and integration of renewable energy.

HEEJIN KIM (Member, IEEE) received the B.S. and Ph.D. degrees in electrical engineering from Yonsei University, Seoul, South Korea, in 2010 and 2015, respectively. He was a Postdoctoral Fellow at Yonsei University, from 2015 to 2019, where he has been a Research Professor, since 2019. Also, he is currently leading the Research Institute of Pion Electric as a CTO. His research interests include modeling and control of power converters, modular multilevel converters, flexible ac transmission systems/high-voltage direct current, power electronic applications in power systems, and integration of renewable energy.

EUN-JAE LEE (Member, IEEE) received the B.S. and M.S. degrees in electrical engineering from Kwangwoon University, in 2008. He is currently working at LS Electric Company Ltd. His research interests include HVDC systems, state estimation, topology identification, and substation automation.

SEUNG-TAEK BAEK (Member, IEEE) received the Ph.D. degree in electrical engineering from Myongji University, Yongin, South Korea, in 2004. Since 2010, he has been working at LS Electric Company Ltd. His current research interests include static power converters for renewable energy and high-voltage direct current (HVDC) systems.

JAE WOONG SHIM (Member, IEEE) received the dual Ph.D. degree in electrical engineering from Yonsei University, Seoul, South Korea, and The University of Sydney, Sydney, NSW, Australia, in 2016. He was a Senior Researcher at the HVDC Research Center, LS Electric Company Ltd., from 2016 to 2017. He worked at the Department of Energy Engineering, Inje University, South Korea, from 2017 to 2021. He has been working with the Department of Electrical Engineering, Sangmyung University, Seoul, since 2021, where he is currently leading the Power System Control and Stability Laboratory. His research interests include power system dynamics and control, HVDC/FACTS/MTDC/MVDC/ESS operation and control, wide-area control with renewables, and power system stability issues with power electronics devices.